GEOPHYSICAL RESEARCH LETTERS, VOL. 13, NO. 1, PAGES 56-59, JANUARY 1986

MINIMUM DETECTABLE POLLUTION LEVELS FROM SATELLITE IMAGERY

A.A. Tsonis[1] and W.R. Leaitch

Atmospheric Environment Service, Downsview, Canada

Abstract. In this paper the detection of haze using satellite imagery is compared with simultaneous aircraft measurements of haze parameters. The vertical optical depths of the effective pollutant layers are compared with results from the satellite data in order to gauge a threshold for the detection of haze from satellites. This comparison indicates that in terms of the optical depth this threshold is approximately equal to 0.065. Regression analysis indicates that a ground aerosol $SO_4^=$ concentration of $\sim 3\ \mu gm^{-3}$ may be typical of such a value of optical depth.

Introduction

The presence and transport of pollutants is a fundamental concern to the issue of acid precipitation and more generally to the health of the environment.

Visual inspection of the Geostationary Orbiting Environmental Satellite (GOES) images has proven beneficial in identifying pollution episodes. An excellent review on satellite detection of pollution episodes is given by Lyons and Dooley (1978) where the feasibility of using digitally processed GOES images to detect the extent and movement of hazy air masses is examined. Their analysis encourages the use of satellite images for such purposes. However, depending upon the pollutant type, its concentration, and the depth of the atmosphere which it occupies, the pollution may not always be identifiable from satellite imagery. The purpose of this paper is to combine aircraft measurements and satellite data in order to gauge a threshold for the detection of haze from satellites.

Data

Two data sets have been used in this study. The first data set consists of GOES visible (0.54 - 0.70 μm wavelength) and thermal infrared (10.5 - 12.6 μm wavelength) sensor images. These images have been digitized with the visible count (C_{VIS}) ranging from 0 - 63 and the infrared count (C_{IR}) ranging from 0 - 255. The spatial resolution of the images is 4 x 4 km and the temporal resolution is 30 minutes. The second set consists of aircraft measurements of the aerosol size distribution (0.1 - 15 μm radius), aerosol chemistry, relative humidity, temperature and other state parameters. The measurements were made over regions of central Ontario, Canada, during July 1982 and January-February 1984 as part of two large scale field experiments investigating atmospheric pollutants. Complete descriptions of the data sets can be found in Tsonis and Isaac (1985) and Isaac et al. (1985).

Data Analysis and Results

The use of the bivariate frequency distributions in the visible/infrared domain has proven very useful in distinguishing various scenes in the satellite images. These frequency distributions, which are actually two-dimensional histograms, are calculated as follows: an area usually 400 x 400 km is selected. Due to digitization, such an area is represented in both images by 100 x 100 points. Each point, depending on the principle reflecting surface (water, land, clouds, etc.), acquires a visible count $0 \leq C_{VIS} \leq 63$ and an infrared count $0 \leq C_{IR} \leq 255$. From this spectral information, the bivariate frequency distribution is then calculated from the number of points whose responses in the visible and infrared fall within certain intervals. Tsonis (1984) and Tsonis and Isaac (1985) have demonstrated that for a cloudless land scene with no visibly apparent pollution and without snow on the ground most of the points in the bivariate frequency distribution are found in the visible interval 20-23. Therefore, for such scenes the frequency distribution will always peak at visible counts greater than or equal to 19 and less than or equal to 23. It should be mentioned that in the above references and here land refers to mainly forestry regions dotted with small lakes. An example of such a distribution is given by the solid lines in Figure 1. These lines are contours of equal frequencies and they are drawn at intervals of 500. They represent the observed frequency distribution in the visible/infrared domain at 1500 GMT on 1 July 1982 from a nonhazy cloudless land scene of size 400 x 400 km centered at 46°N and 79°W.

The effect of haze is to increase the atmospheric albedo. Therefore, if haze is introduced to cloudless land scenes and if haze is "sensed" by the satellite then the frequency distribution should be shifted towards higher visible responses. The above is effectively demonstrated in Figure 1 by the dashed contours which represent the observed frequency distribution at 1630 GMT on 23 February 1984 of a hazy cloudless scene of size 400 x 400 km centered again at 46°N and 79°W. The average temperature of this area on 1 July 1982 is 8°C higher than that on 23 February 1984. To elucidate effects of haze in the infrared the

1 Present affiliation:
Dept. of Geological and Geophysical Sciences
The University of Wisconsin-Milwaukee
Milwaukee, Wisconsin 53201

Paper number 5L6684.
0094-8276/86/005L-6684$03.00

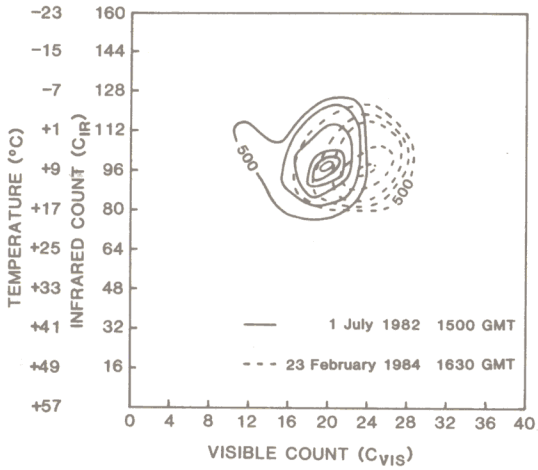

Fig. 1. Contour representation of the bivariate frequency distribution in the visible and infrared space for 1 July 1982 at 1500 GMT (solid contours) and for 23 February 1984 at 1630 GMT (dashed contours).

distribution on 1 July 1982 has been shifted in Figure 1 towards lower temperatures by 8°C. Such an operation centers both distributions at similar infrared levels. The effect of haze in the infrared is, as expected, minor compared to the effect of haze in the visible. The average temperature and the hazy and nonhazy classification are determined by observations of the ground synoptic stations within this area. All of these stations report high visibility for 1 July 1982 whereas all of them report low visibility and haze for 23 February 1984.

The presence of clouds results in higher visible and infrared counts, but when the cloud amount is smmall (i.e. < 3/10) they do not, in general, generate a peak (Tsonis, 1984). In such cases and for nonhazy atmospheres the resulting frequency distribution retains the peak due to the cloudless land scene, but its spread towards higher visible and infrared responses is now more pronounced. In cases where a peak due to a field of scattered clouds is generated it will be located at $C_{VIS} > 23$ and it could be mistaken as representing haze due to similar observed visible responses. Since the effect of haze in the infrared is minor by comparison with the visible, the infrared information can be used to discriminate between colder clouds and warmer haze. When the amount of cloud increases then the situation becomes rather obscured because when clouds dominate the scene, information about the underlying haze is suppressed. The ability of the satellite to sense pollution should, therefore, be tested in mostly clear skies conditions.

All aircraft data were collected in flights which were confined to a 400 x 400 km area centered over North Bay (46°N, 79°W), Ontario. For this paper only days with average cloud amounts (as specified by the reports of the synoptic stations within the area of interest) less than 3/10 have been considered. The selected days and flight times are shown in Table 1. The employed satellite data were taken at a time (T_s) to best match the time of the aircraft measurements. Then, for each day, the bivariate frequency distribution in the visible/infrared domain is produced. If the peak's visible count (Vp) is less than or equal to 23, then the satellite classification (S.C.) is nonhazy. Otherwise the day is classified as hazy. All the above information is given in Table 1. 6 February 1984 is the only day with snow on the ground. In cases such as this, even without pollution, the bivariate distribution will always peak at $C_{VIS} > 23$. From our experience with satellite imagery we have never observed a case where the peak's visible count exceeds a value of 35 for cloudless nonhazy atmospheres with snow on the ground. Based on this and for the sake of a larger sample we have decided to include this case.

One may observe that 1 July 1982 is not included in the selected days. The reason for this is that aircraft measurements were not collected on that day. The purpose of Figure 1 was to demonstrate as clearly as possible the effect of haze in the visible. The choice of 1 July 1982 and 23 February 1984 was based on the simplicity, similarity and clear separation between their bivariate frequency distributions.

Subsequently, for each day the vertical optical depth due to the presence of the pollutant layer has been estimated using aircraft profiles of the aerosol particle size distribution and relative humidity. Two instruments were used to measure the aerosol spectra; an ASASP-100X (Active Scattering Aerosol Spectrometer Probe) and an FSSP (Forward Scattering Spectrometer Probe). Calibrations of this particular ASASP, using nearly monodisperse NaCl and latex particles suggest that the probe sizes particles between 0.09 and 1.0 μm radius. This is supported by the findings of Pinnick and Auvermann (1979). It has also been determined that heating mechanisms within the probe dry the particles, before detection, in atmospheres with relative humidities < 100%. In the case of the FSSP the particle configuration is not altered before detection. The sizing calibration used in this study for the FSSP can be found in Dye and Baumgardner (1985).

The optical depth (τ) has been calculated from:

$$\tau = \sum_j \left(\sum_i N_i \cdot Q_i \cdot r_i^2 \cdot \pi \right) \cdot L_j \quad (1)$$

where N_i is the number of aerosol particles in a size class specified by the radius r_i, Q_i is the scattering efficiency of the particle of radius

Table 1. Selected days, flight times and results of the satellite classification.

DAY	FLIGHT TIME (GMT)	T_s (GMT)	Vp	S.C.
6 July 82	1800-1830	1800	25	hazy
16 July 82	1900-1930	1900	26	hazy
17 July 82	1900-2020	1930	26	hazy
19 July 82	1900-1920	1900	21	nonhazy
15 Feb. 84	1900-1930	1900	21	nonhazy
22 Feb. 84	1500-1600	1530	22	nonhazy
23 Feb. 84	1520-1500	1530	24	hazy
*6 Feb. 84	1600-1700	1630	37	hazy

*snow on the ground

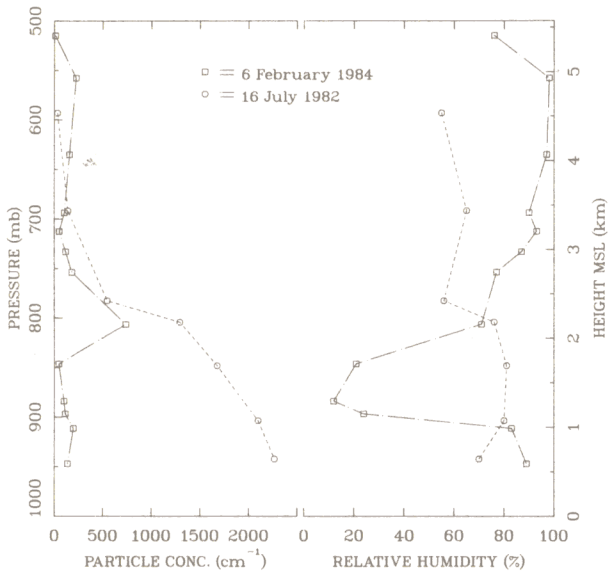

Fig. 2. Examples of aircraft measurements of aerosol particle concentrations and relative humidity as a function of pressure for 16 July 1982 and 6 February 1984.

r_i and Lj is the thickness of the jth layer of the atmosphere.

The thickness of the layers (Lj) is arbitrarily determined based upon the vertical gradient in the aerosol size spectra and the relative humidity. Two examples of measurements, from 16 July 1982 and 6 February 1984 are given in Figure 2 illustrating the vertical gradients of aerosol particles concentration and relative humidity.

Mie scattering computations were employed to determine the value of Q_i for the solar radiation (0.55μm wavelength). For the supermicron particles (FSSP) the values of N_i and r_i are specified directly as measured. The index of refraction is assumed to be 1.4 (nonabsorbing) because it is not known how hygroscopic these particles were and/or how much water was in the composition of the aerosol. Although the sizing calibration used with the FSSP is based upon spheres of water, differences between the FSSP scattering responses for indices of refraction of 1.33 and 1.4 are negligible in terms of this discussion. For the submicron (ASASP) particles, N_i is specified directly from the measurements. The measured radius, however, is incremented by some fraction according to the assumed water soluble fraction of the aerosol and according to the measured relative humidity (frequently > 70%) and the results of Tang and Munkelwitz (1977). Aerosol composition measurements have indicated that the water soluble fraction of the submicron aerosol can be generally represented by NH_4HSO_4. The index of refraction of the submicron particles was varied between 1.47 (i.e. NH_4HSO_4) and 1.33 (H_2O) based upon the incremented volume fraction. Calculations were performed for two possible water soluble volume fractions: 50% and 100%. These represent approximate range values based on the work of Isaac et al. (1985) on the same aircraft data set. The optical depths determined for each day and for the two cases are given in Table 2 as τ_{50} and τ_{100} (i.e. for 50% and 100% water soluble fractions, respectively).

Table 2. Computed optical depths for each case studied.

DAY	τ_{100}	τ_{50}
6 July 82*	0.344	0.233
16 July 82*	0.560	0.345
17 July 82*	0.420	0.251
19 July 82	0.036	0.027
15 Feb. 84	0.021	0.014
22 Feb. 84	0.077	0.047
23 Feb. 84*	0.120	0.080
6 Feb. 84*	0.400	0.200

In Table 2, the star in the first column indicates the days that according to satellite have been classified as polluted (from Table 1). According to the results in Table 2 the minimum τ_{100} associated with a day that is classified as polluted by the satellite is 0.120. At the same time the maximum τ_{100} for a classified nonpolluted day is 0.077. One could, therefore, argue with some confidence that for a 100% water soluble fraction the minimum detectable pollution levels from satellite imagery are associated with a value of optical depth ~0.1. Similarly for a 50% water soluble fraction one could argue that the minimum detectable pollution levels are associated with a value of optical depth ~0.065.

Isaac et al. (1985) have shown that the volume water soluble fraction tends to be lowest for the conditions of least pollution. Therefore, the value of τ_{50} is more appropriate, than that of τ_{100}, when considering a threshold value.

It should be mentioned, at this point, that the applicability of the measured optical depth to a 400 x 400 km area is, in general, warranted. This is supported by the pollution measurements of the ground stations during the experimental period which indicate (especially

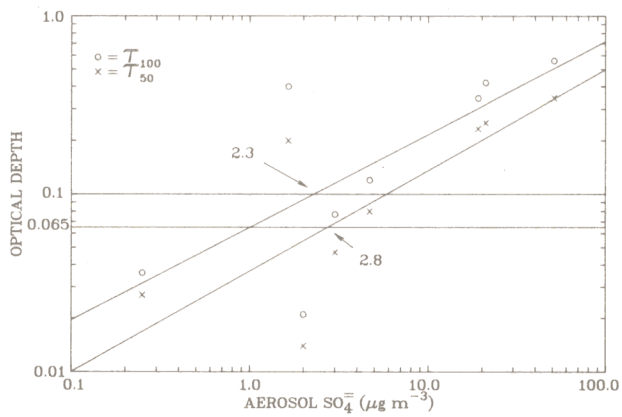

Fig. 3. Calculated optical depth due to aerosol as a function of the concentration of aerosol sulphate ($SO_4^=$) measured at the ground. Circles indicate the value of the optical depth assuming a 100% water soluble volume fraction for the aerosol, while the x's indicate the corresponding optical depth when the aerosol is assumed to be only 50% water soluble by volume.

for mostly clear skies situations) that the pollution episodes were fairly homogeneous.

In Figure 3, the variation of the optical depth (as τ_{100} and τ_{50}) as a function of the measured concentration of aerosol $SO_4^=$ at ground level is illustrated. The Spearmen rank correlation between the τ_{100} and $[SO_4^=]$ values is 0.81. The same correlation is obtained between the τ_{50} and $[SO_4^=]$ values. Such a high value would indicate a strong linear dependence between optical depth and ground level $[SO_4^=]$. The regression lines of log $[SO_4^=]$ on logτ_{100} and log $[SO_4^=]$ on logτ_{50} are also shown. They intercept the $\tau = 0.1$ line at $[SO_4^=] = 2.3\ \mu gm^{-3}$ and the $\tau = 0.065$ line at $[SO_4^=] = 2.8\ \mu gm^{-3}$, respectively. These results indicate that the satellite is very effective in detecting pollution (a $[SO_4^=] < 3\ \mu gm^{-3}$ or so can be regarded as a relatively mild pollution episode). Simulations performed for a dry atmosphere (not shown) indicate that more of the variation in optical depth is explained by the concentration of aerosol $SO_4^=$ measured at the ground.

Conclusions

We have combined, in a unique way, aircraft and satellite data in order to determine the minimum detectable pollution levels from GOES imagery. For the region of study it was found that in terms of the optical depth of the effective pollutants layer the minimum detectable pollution is associated with $\tau \sim 0.065$. This value of τ corresponds to mild pollution episodes and therefore it is concluded that the satellite is very effective in detecting pollution. Regression analysis suggested that a ground aerosol $SO_4^=$ concentration of 3 μgm^{-3} may be typical for this value of τ. The results are representative of the experimental area and may not be directly applicable to other areas where the background albedo and/or aerosol properties are different. However, the results reported here given the first quantitative evaluation of the ability of the GOES satellite in detecting pollution and could be useful to researchers that use these or similar satellite data to study and verify long range pollution transport, the dispersion of pollutants and the important problem of acid precipitation.

Acknowledgements. Many scientists and technicians from the Atmospheric Environment Service and the National Aeronautical Establishment assisted in collecting the aircraft data for this work. Specifically we wish to thank J.W. Strapp and M. Wasey. We also wish to thank M.D. Couture for programming assistance and M. Kleiber for typing the manuscript.

References

Dye, J.E. and D. Baumgardner, Evaluation of the forward scattering spectometer probe. Part I: electronic and optical studies, J. Atmos. Oceanic Technol., 1, 329-344, 1984.

Isaac, G.A., W.R. Leaitch, J.W. Strapp, and K.G. Anlauf, Summer aerosol profiles over Algonquin park, Canada, Atmospheric Environment, in press, 1985.

Lyons, W.A. and J.C. Dooley, Jr., Satellite detection of long-range pollution transport and sulphate aerosol haze, Atmospheric Environment, 12, 621-631, 1978.

Pinnick, R.G. and H.J. Auvermann, Response characteristics of Knollenberg light-scattering aerosol counters, J. Aerosol Sci., 10, 55-74, 1979.

Tang, I.N. and H.R. Munkelwitz, Aerosol growth studies - III Ammonium bi-sulfate aerosols in a moist atmosphere, J. Aerosol Sci., 8, 321-330, 1977.

Tsonis, A.A., On the separability of various classes from the GOES visible and infrared data, J. Climate Appl. Meteor., 23, 1392-1410, 1984.

Tsonis, A.A. and G.A. Isaac, On a new approach for instantaneous rain area delineation in the midlatitudes using GOES data, J. Climate Appl. Meteor., 24, 1208-1218, 1985.

W.R. Leaitch
Atmospheric Environment Service
4905 Dufferin Street
Downsview, Ontario, Canada
M3H 5T4

A.A. Tsonis
Geological and Geophysical Sciences
The University of Wisconsin-Milwaukee
Milwaukee, Wisconsin 53201

(Received August 27, 1985;
revised November 4, 1985;
accepted November 5, 1985.)